CCR2 Signaling Promotes Brain Infiltration of Inflammatory Monocytes and Contributes to Neuropathology during Cryptococcal Meningoencephalitis

Jintao Xu,[a,b] Anutosh Ganguly,[a,c] Jessica Zhao,[a,b] Michel Ivey,[a] Rafael Lopez,[a] John J. Osterholzer,[a,b] Clifford S. Cho,[a,c] 🔟 Michal A. Olszewski[a,b]

aResearch Service, Ann Arbor VA Health System, Department of Veterans Affairs Health System, Ann Arbor, Michigan, USA
bDivision of Pulmonary and Critical Care Medicine, Department of Internal Medicine, University of Michigan Health System, Ann Arbor, Michigan, USA
cDivision of Hepatopancreatobiliary and Advanced Gastrointestinal Surgery, Department of Surgery, University of Michigan, Ann Arbor, Michigan, USA

ABSTRACT Cryptococcal meningoencephalitis (CM) is a leading cause of central nervous system (CNS) infection-related mortality worldwide, with surviving patients often developing neurological deficiencies. While CNS inflammation has been implicated in the pathogenesis of CM, little is known about the relative contribution of the specific inflammatory/immune pathways to CNS pathology versus fungal clearance. Increased cerebrospinal fluid level of C-C chemokine receptor 2 (CCR2) ligand CCL2 is associated with disease deterioration in patients with CM. Using a murine model, we investigated the role of the CCR2 pathway in the development of CNS inflammation and pathology during CM. We found that CCR2-deficient mice exhibited improved 28-day survival and alleviated neurological disease scores despite a brain fungal burden higher than that of the WT mice. Reduced CM pathology in CCR2-deficient mice was accompanied by markedly decreased neuronal cell death around cryptococcal microcysts and restored expression of genes involved in neurotransmission, connectivity, and neuronal cell structure in the brains. Results show that CCR2 axis is the major pathway recruiting $CD45^{hi}CD11b^+Ly6C^+$ inflammatory monocyte to the brain and indirectly modulates the accumulation of $CD4^+$ T cells and $CD8^+$ T cells. In particular, CCR2 axis promotes recruitment of interferon gamma (IFN-γ)-producing $CD4^+$ T cells and classical activation of myeloid cells. In this context, CCR2 deletion limits the immune network dysregulation we see in CM and attenuates neuropathology. Thus, the CCR2 axis is a potential target for interventions aimed to limit inflammatory CNS pathology in CM patients.

IMPORTANCE Cryptococcal meningoencephalitis (CM) causes nearly 200,000 deaths worldwide each year, and survivors frequently develop long-lasting neurological sequelae. The high rate of mortality and neurologic sequelae in CM patients indicate that antifungal therapies alone are often insufficient to control disease progression. Here, we reveal that CM disease progression in mice is accompanied by inflammatory monocytes infiltration at the periphery of the infected foci that overlap locally perturbed neuronal function and death. Importantly, we identified that CCR2 signaling is a critical pathway driving neuroinflammation, especially inflammatory monocyte recruitment, as well as CNS pathology and mortality in CM mice. Our results imply that targeting the CCR2 pathway may be beneficial as a therapy complementary to antifungal drug treatment, helping to reduce CNS damage and mortality in CM patients.

KEYWORDS CCR2, cryptococcal meningoencephalitis, central nervous system infections, immunopathogenesis, inflammatory monocyte

The fungal pathogen *Cryptococcus neoformans* is a common cause of adult meningoencephalitis in many parts of the world, resulting in nearly 200,000 deaths worldwide each year (1, 2). Cryptococcal meningoencephalitis (CM) is not only characterized by a high mortality rate (up to 30 to 50%) (3, 4), but survivors frequently develop long-lasting severe neurological sequelae, including memory loss, vision deficiencies, hearing and speech impairments, and motor deficits (2, 5). Recent studies revealed that inflammation triggered in response to *Cryptococcus* rather than the pathogen itself can lead to neuropathology in a subset of HIV$^+$ and HIV$^-$ CM patients (2, 6–9). Thus, selective control of the pathological immune pathways may become an important element of therapies aimed at preventing the immune-mediated damage within the CNS.

While required for anticryptococcal defenses, CD4$^+$ T cells have emerged as critical drivers of immunopathology in both human and murine CM (10–13). Rapid reconstitution of T cells in HIV$^+$ CM patients by antiretroviral therapy (ART) can lead to immune reconstitution inflammatory syndrome (c-IRIS), characterized by a dysregulated T cell response (14). Likewise, noncompromised CM patients often develop severe neurological pathology that is steroid responsive (6). CD4$^+$ T cells also orchestrate lethal immune pathology in animal models (12, 13, 15). However, CD4$^+$ cells do not perform their immune functions on their own but require antigen-presenting cellular partners to become activated and to execute their effector functions in neuroinflammatory diseases (16). Myeloid cells, especially recruited monocytes and monocyte-derived cells, exacerbate pathological T cell responses, for example, by secreting chemokines to recruit T cells and by stimulating their antigen-specific cytokine production (16–18). At the same time, upon activation by the T cells, these cells can produce cytotoxic molecules, such as reactive oxygen species known to cause collateral tissue damage (17, 18). CD45^{high}Ly6C$^+$CD11b$^+$ inflammatory monocytes (IM) are recruited in the CNS during CM (13, 19, 20), but their function and mechanisms responsible for their recruitment remain unclear.

CC chemokine receptor 2 (CCR2) is the major chemokine receptor required for monocyte migration from bone marrow to the inflammatory sites through binding CC chemokine ligands such as CCL2 (21). The role of CCR2 signaling in pulmonary cryptococcal infections is predominantly protective by promoting protective Th1 antifungal immunity over nonprotective Th2 (22–25). However, in already Th2-biased response to *C. neoformans*, CCR2$^+$ IM can mediate pathological effects in the lungs (26). Specific roles of the CCR2 pathway remain less defined in the CNS during CM. Previous studies showed that CCL2 is elevated in the cerebrospinal fluid of CM patients and linked to the development of brain pathology (6, 19). Thus, we hypothesize that the CCL2/CCR2 pathway modulates CNS inflammation and contributes to inflammatory pathology in CM.

Here, using a murine model of CM, we found that the CCR2 pathway drives fatal pathology even though it contributes to the fungal clearance. CCR2$^{-/-}$ CM mice are largely protected from neurological deterioration and mortality. Improved CM outcomes in CCR2$^{-/-}$ mice were marked by reduced neuronal cell death and restored gene expressions related to neurotransmission. Accumulation of CD11b$^+$Ly6C$^+$ IM, the major myeloid population infiltrating the brain during CM, depended almost entirely on CCR2 signaling. CCR2 modulates the accumulation and ultra-Th1 polarization of CD4$^+$ T cells previously demonstrated to be pathological during CM. Our results suggest that therapeutic strategies targeting the CCR2 pathway could reduce neuronal pathology during severe CM.

RESULTS

CCR2 deficiency improves animal survival despite decreased fungal clearance during CM. Elevated CCL2 in the cerebrospinal fluid of patients with HIV-associated CM predicts the risk of immune reconstitution inflammatory syndrome, linking overactivated CCL2/CCR2 axis with the development of inflammatory brain pathology (19). CCR2-dependent entry of IM into the CNS contributes to immunopathology in several
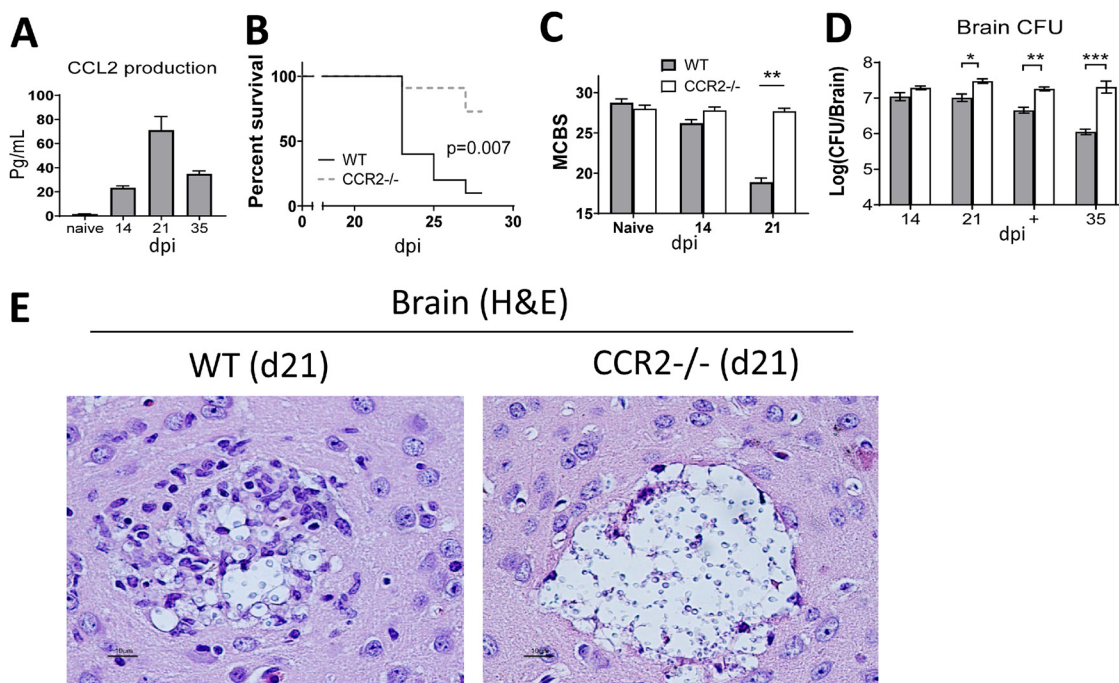
FIG 1 CCR2 drives immunopathology and mortality during CM. C57BL/6J mice were infected with 10^6 CFU of *C. neoformans* 52D via retro-orbital intravenous inoculation. (A) Production of chemokine CCL2 in the brain homogenate at various time points was evaluated by CBA assay. (B) $CCR2^{-/-}$ mice showed prolonged survival and lower mortality than that of the WT-infected mice ($n = 10$). (C) MCBS scores of infected WT and $CCR2^{-/-}$ mice were compared to evaluate the overall health and neurological status. $CCR2^{-/-}$ mice exhibited less-severe CM symptoms. (D) Brain fungal burdens were calculated on 14, 21, postdeath (+), and 35 dpi. CCR2 deficiency significantly impairs fungal control in the brain. We did not observe any significant difference in brain CFU, as well as CNS inflammation. (E) Brains from perfused WT and $CCR2^{-/-}$ mice were paraffin-embedded, coronal sectioned, stained with hematoxylin and eosin (H&E), and imaged at $(40\times)$. Note that stained *C. neoformans* organisms occupy a relatively small area in the WT compared to that of CCR2-deficient mice and that *C. neoformans* are better contained and surrounded by the leukocyte infiltrate in WT mice but occupy a largely extracellular zone in $CCR2^{-/-}$ mice. Data shown are the mean ± standard error of the mean (SEM) from an experiment representative of two independent experiments ($n > 4$). **, $P < 0.01$; ***, $P < 0.001$.

neurological diseases (27–29). We thus evaluated the function of the CCL2-CCR2 axis in the pathological process of CM using our murine model, which reproduces human neuronal pathology associated with severe CM (12, 13). We found a significantly elevated level of CCL2 during CM, which began to increase at 14 days postinfection (dpi) and peaked at 21 dpi (Fig. 1A). The sharp increase in CCL2 expression marked the onset of mouse mortality post 21 dpi (Fig. 1B). About 80% of animals succumbed to infection between 21 and 30 dpi in wild-type (WT) mice. However, $CCR2^{-/-}$ mice showed substantially improved survival, with only 25% mortality noted before 30 dpi (Fig. 1B). Unlike the WT mice, the infected $CCR2^{-/-}$ mice did not develop severe neurological and behavioral defects, as quantified per murine coma and behavior scale (MCBS) (Fig. 1C). Strikingly, improved survival and behavioral readouts in $CCR2^{-/-}$ mice were accompanied by a fungal load in the brain 2- to 3-fold higher than that in WT mice at 21 dpi and at the time of euthanasia (Fig. 1D). We did not observe significant differences in CFU, survival, or MCBS scores between animal sexes, and data from both sexes were included in the figures. Histological analysis showed more and larger cryptococcal clusters in the brains of $CCR2^{-/-}$ mice compared to those in the brains of WT mice at 21 dpi (Fig. 1E and see Fig. S1 in the supplemental material). However, cryptococcal microcysts in the WT mice were encircled by cellular inflammatory infiltrates, which were largely absent from the edges of cysts in $CCR2^{-/-}$ brains (Fig. 1E). Thus, despite benefiting fungal clearance, the CCR2 axis contributed to severe CM symptoms and mortality that correlate with pathological evidence of brain inflammation.

CCR2 deletion rescues neuronal cell dysfunction and apoptosis during CM. To establish molecular processes that accompany brain pathology during CM, we measured
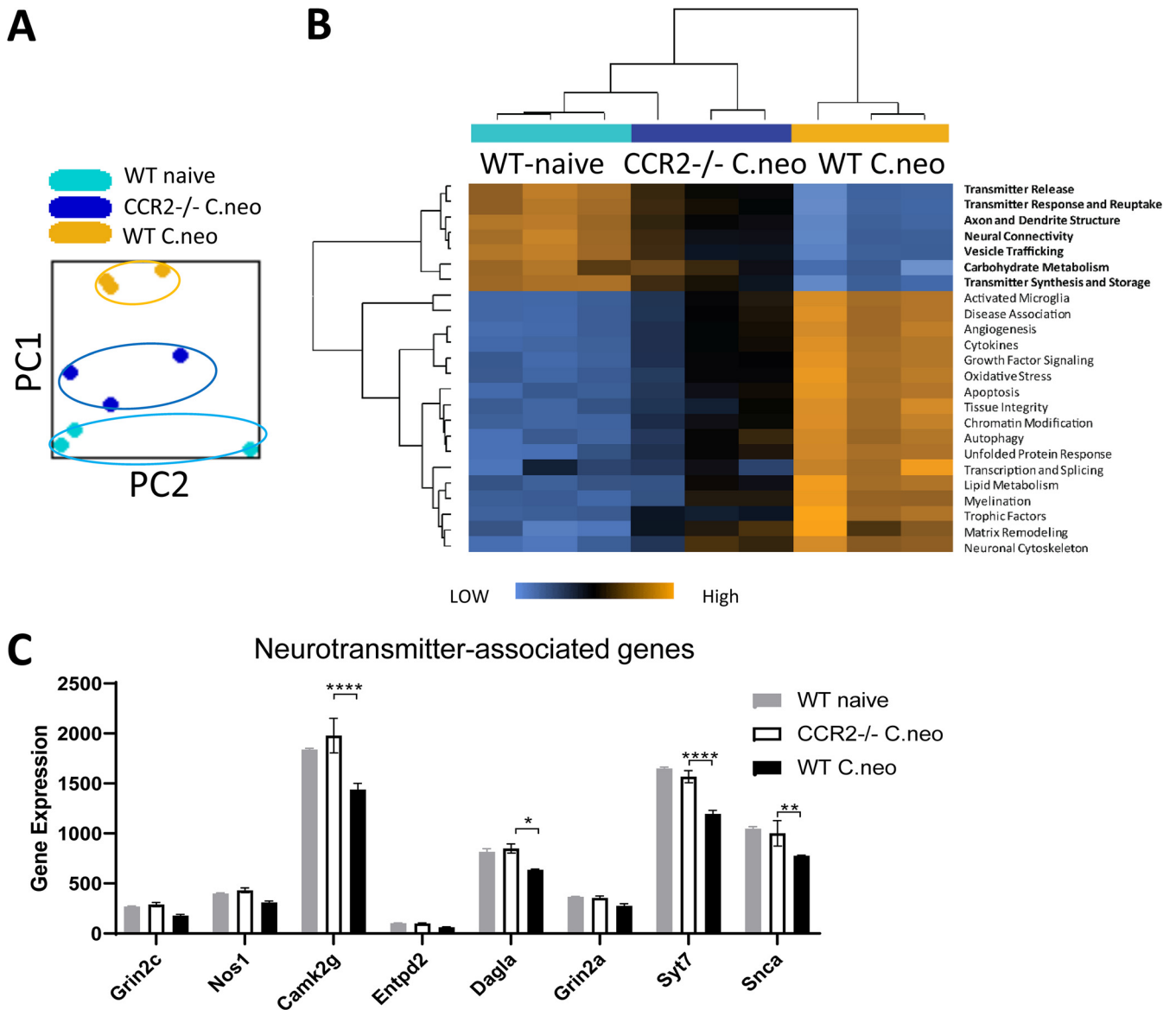
FIG 2 CCR2 contributes to dysregulated gene expression in neurotransmission pathways during CM. Gene transcripts of brain homogenates from naive and infected WT and infected CCR2$^{-/-}$ at 21 dpi were analyzed using a NanoString multiplex neuropathology panel. (A) Principal-component analysis of normalized read counts of the total 700 transcripts associated with neuropathology. Infected WT control and infected CCR2$^{-/-}$ mice formed separate clusters along with principal components 1 and 2. Data from NanoString shown are from one experiment with $n = 3$ samples per group, and each sample was pooled from 3 mice. (B) CCR2 deletion ameliorated the neurodegeneration and neuroinflammation pathway scores altered by CM in the WT mice. In particular, CCR2 deficiency preserved the overall pathways associated with neurotransmission and decreased expression of genes associated with neuroinflammation (activated microglia, cytokines), metabolism (autophagy, lipid metabolism, oxidative stress, transcription and splicing, unfolded protein response), and cell structure integrity (neural connectivity, neuronal cytoskeleton, tissue integrity). (C) Expression of selected genes associated with neurotransmission, *GRIN2C*, *NOS1*, *CAMK2G*, *ENTPD2*, *DAGLA*, *GRIN2A*, *SYT7*, and *SNCA*, was shown. Note that CM induced suppression of these genes in the brain of the WT mice but not in that of CCR2-deficient mice. Bars show mean ± SEM ($n = 3$), *, $P < 0.05$; **, $P < 0.01$; ****, $P < 0.0001$.

changes in mRNA transcripts using a NanoString neuropathology multiplex panel, which measures the expression of 700 genes associated with six fundamental pathways: neuro-transmission, neuron-glia interactions, neuroplasticity, cell structure integrity, neuroinflammation, and metabolism. We measured the effect of CCR2 deletion on the development of these molecular signatures at 21 dpi, the peak of CNS inflammation during CM. Principal-component analysis of normalized gene transcript read counts consistently showed that the uninfected WT mice, infected WT mice, and infected CCR2$^{-/-}$ mice formed separate clusters by principal components 1 and 2 (Fig. 2A). The CCR2$^{-/-}$ mice with CM clustered between the infected and naive WT mice and closer to the uninfected mice. Analysis of specific pathway scores showed that CM resulted in a significant reduction of

transcriptional signatures for physiological neurotransmission function (transmitter release, transmitter response and reuptake, transmitter synthesis and storage, vesicle trafficking) and carbohydrate metabolism relative to those of the uninfected brains (Fig. 2B). Concurrently, scores of pathways involved in neuroinflammation (activated microglia, cytokines), neurodegeneration and metabolic stress responses (autophagy, apoptosis, lipid metabolism, oxidative stress, transcription and splicing, unfolded protein response), and repair responses (neural connectivity, neuronal cytoskeleton, tissue integrity) increased significantly postinfection (Fig. 2B). CCR2 deletion largely prevented dysregulation in these pathways during CM, showing limited changes or resembling naive mice (Fig. 2B). Quantification of selected transcripts associated with neurotransmission, including *camk2g*, *dagla*, *syt7*, and *snca*, showed that CCR2 deficiency restored their suppressed expression (Fig. 2C). In addition to neuronal function genes, we analyzed the expression of transcriptional signatures of main resident cells known to be affected by and contribute to the inflammatory process within the CNS. CM significantly reduced oligodendrocyte and astrocyte but enriched microglia and endothelial cell transcriptional signatures in the WT mice (Fig. S2). In the infected $CCR2^{-/-}$ mice, we observed that these effects of CM on cell signature scores were only partial (oligodendrocyte and microglia) or not present (astrocyte and endothelial cell) (Fig. S2), supporting that in the course of CM, CCR2 signaling affects the status of both neuronal and other CNS resident cells.

Because of the very focal nature of the infection and inflammatory infiltrates in CM, the suppression of the neurotransmission gene expression measured in the global brain RNA may appear relatively modest (~20% decrease) (Fig. 2C). However, these changes were highly significant, motivating our *in situ* quantitation of the selected markers at the perimeter of the individual cryptococcal lesions. We stained CNS sections from WT and $CCR2^{-/-}$ mice for synaptic vesicle protein synaptotagmin-7 (Syt7), one of the top differentially expressed genes involved in neurotransmission pathways by our NanoString analysis. We found a uniform distribution of parallel neuronal cells (identified by β-III tubulin) with intracellular Syt7 expression, as well as extracellular Syt7, as evidence of postsynaptic vesicle release in both the uninfected WT and $CCR2^{-/-}$ mice (Fig. S3). However, expressions of Syt7 and β-III tubulin at the perimeter of the cryptococcal microcysts were profoundly reduced in the infected WT mice relative to those in the infected $CCR2^{-/-}$ mice (Fig. 3A), suggesting a severe defect in neurotransmission and loss of neuron cells. We further used cleaved caspase-3 (a marker of apoptosis) in β-III tubulin positive cells to measure potential neuronal death. In naive mice, β-III tubulin staining marked bundles of neurons in which cleaved caspase-3 signal was completely absent (Fig. S3). However, the cleaved caspase-3 fluorescence was high and colocalized with neurons at 21 dpi in the brains of the infected WT mice (Fig. 3B). Importantly, the level of the cleaved caspase-3 signal was minimal in the neurons of the infected $CCR2^{-/-}$ mice (Fig. 3B). Together, we conclude that neurological symptoms and CNS pathology in CM manifest neuronal dysfunction and apoptotic death caused by the local inflammatory response, fueled by the CCR2 axis.

C. neoformans brain infection induces massive IM infiltration that depends on CCR2. Studies with pulmonary cryptococcal infection defined that CCR2 plays a critical role in the egress of monocytes from bone marrow, which in the lungs differentiate into effector IM eliminating *C. neoformans* (22, 23, 30). To assess the role of CCR2 in inflammatory cell recruitment during CM, we first evaluated the expression of CCR2 by brain leukocytes. We found that CCR2 was expressed on the surface of $CD45^{hi}CD11b^+Ly6C^+$ IM (Fig. 4A and gating strategy in Fig. S4) but not microglia ($CD45^{low}CD11b^+$) or T cells ($CD45^{hi}CD3^+$) (Fig. 4B). CCR2 gene deletion abolished IM accumulation by 95% in the brain of CM mice at 21 dpi (Fig. 4C), suggesting an essential role of the CCR2 axis in IM accumulation in the brain during CM. Our fluorescence microscopy further showed that the accumulation of $CD11b^+$ myeloid cells around the cryptococcal microcysts also depended on CCR2 signaling (Fig. S5). Systemically, infected $CCR2^{-/-}$ mice showed a decreased frequency of splenic $CD11b^+Ly6C^+$ monocytes but not $CD4^+$ T cells and $CD8^+$ T cells in the
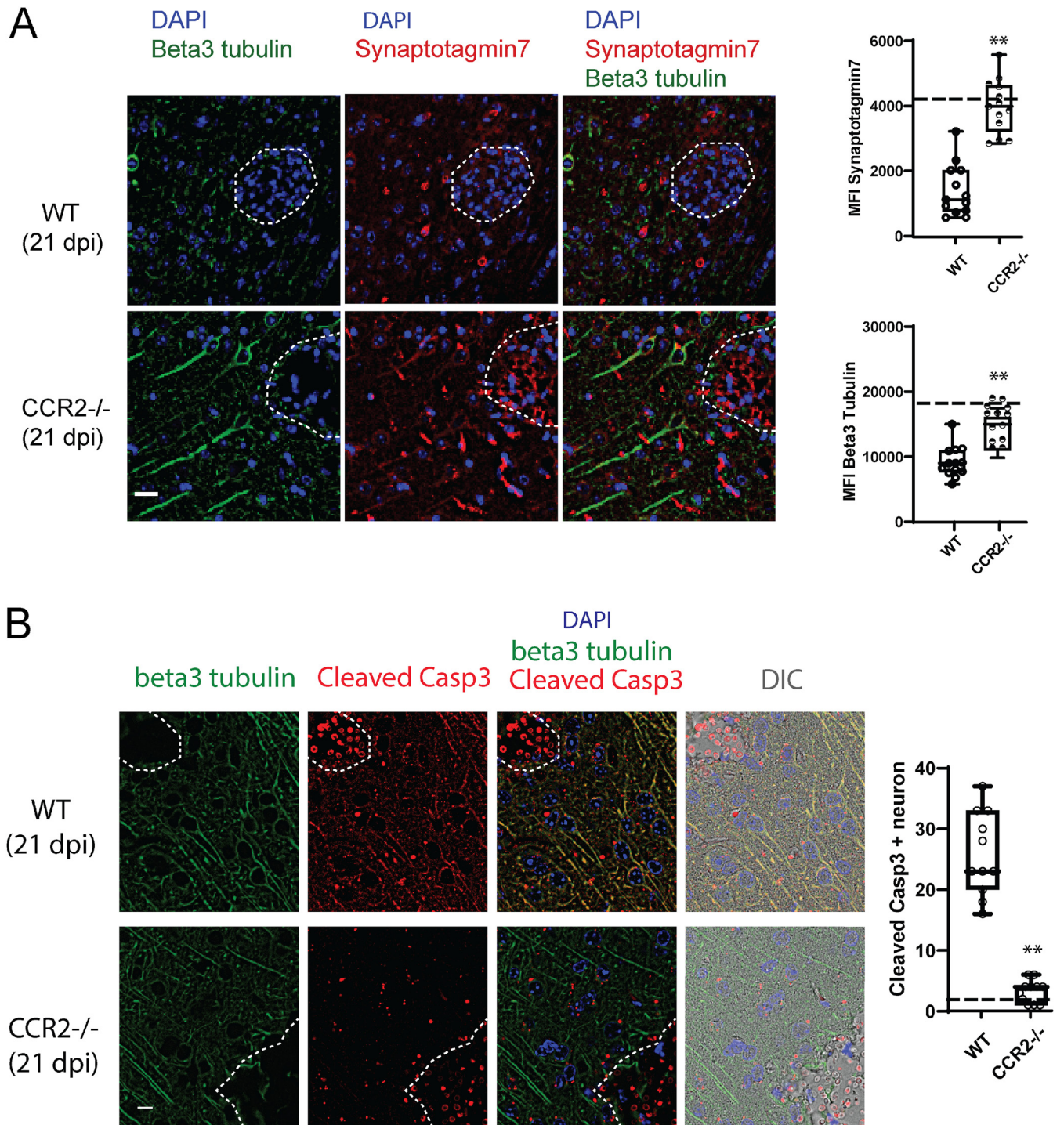
FIG 3 CCR2 pathway promotes regional defects in the production of neurotransmission proteins and neuronal cell apoptotic death. (A) Immunohistochemistry of the brain sections stained with antibodies to beta III tubulin (green) and synaptotagmin-7 (red). In the infected WT mice, neuronal damage was significant in the vicinity of the cryptococcal clusters, with weaker and less-organized beta III tubulin and synaptotagmin-7 signals. In the infected CCR2$^{-/-}$ mice, neuronal damage in the vicinity of the cryptococcal clusters was limited. Dotted lines define the *Cryptococcus* lesions in the brain. The bar graphs on the right show the quantitation of the beta III tubulin and synaptotagmin-7 in the respective conditions, with dashed lines showing the corresponding signals from uninfected mice. Scale bar, 10 μm; magnification, 200×. (B) Immunohistochemistry of brain section stained with antibodies to beta III tubulin (green) and cleaved caspase-3 (red). In infected WT mice, cleaved caspase-3 and beta III tubulin overlay, indicative of dying neurons. In infected CCR2$^{-/-}$ mice, signals of cleaved caspase-3 were minimal. Dotted lines define the *Cryptococcus* lesions in the brain. The bar graph on the right shows the quantitation of the cleaved caspase-3-positive neurons in the respective conditions, and dashed lines show the corresponding signals from uninfected mice. Scale bar, 5 μm; magnification, 600×. DIC, differential interference contrast. The data shown in A and B were from an experiment representative of two independent experiments ($n = 2$ mice per group), and at least 10 fields were examined for each sample.
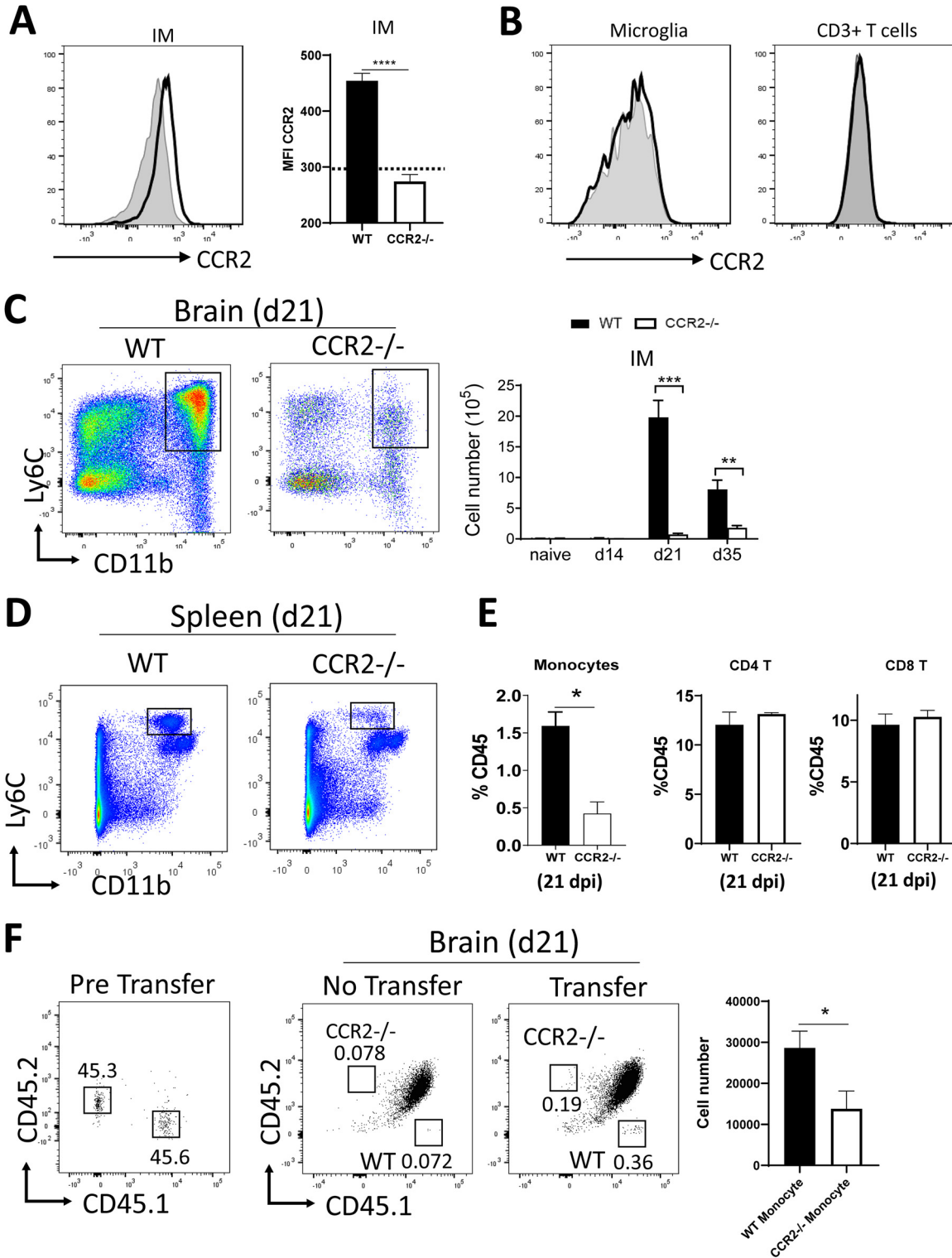
FIG 4 CCR2 pathway is essential for the accumulation of inflammatory monocytes (IM) in the *C. neoformans*-infected brain. Brain leukocytes from WT and CCR2$^{-/-}$ mice were isolated and analyzed. (A and B) CCR2 is mainly expressed by IM but not microglia and T cells in the brain during CM. The gray area in the flow plot and dotted line in the bar graph represent the signal from isotype control. (C) Accumulation of Ly6C^{+}CD11b^{+} IM in the infected brain at days 0, 14, 21, and 35 was evaluated. IM were absent until 14 dpi and showed peak accumulation on 21 dpi in WT mice. Note there was a profound reduction in the total number of IM in the brain of CCR2$^{-/-}$ mice compared to that in the WT mice. (D and E) The frequencies of CD11b^{+}Ly6C^{+} monocytes as well as CD4^{+} T cells and CD8^{+} T cells in spleens of WT and CCR2$^{-/-}$ mice at 21 dpi. (F) Sorted monocytes from WT (CD45.1) or CCR2$^{-/-}$ (CD45.2) mice were mixed at a 1:1 ratio and confirmed by flow cytometry (left panel) and then injected into WT (CD45.1 × CD45.2) recipients at 20 dpi. Frequency and the total numbers of WT and CCR2$^{-/-}$ donor monocytes in the brain of recipient mice were analyzed by flow cytometry

(Continued on next page)

spleens compared to those of WT mice (Fig. 4D and E), consistent with findings observed in our studies of cryptococcal lung infection, in which CCR2 was shown to mediate mainly Ly-6C^{high} monocyte egress from the bone marrow (22, 23).

To further determine if CCR2 was involved in monocyte trafficking from blood to CNS, we performed competitive adoptive transfers. Isolated monocytes from the bone marrow of WT CD45.1 and CCR2$^{-/-}$ CD45.2 mice were cotransferred into WT CD45.1 × CD45.2 mice at 20 dpi. After 24 h posttransfer, we found that CCR2-deficient monocytes migrated into the brain of the recipient mice with 50% efficiency relative to that of the WT monocytes (Fig. 4F), demonstrating that CCR2 signaling contributes to monocyte recruitment from the blood into the brain. Taken together, we found that CCR2 is required for both monocyte egress from bone marrow and monocyte trafficking across the blood-brain barrier during CM.

CCR2-gene deletion curtails neuroinflammation in the *C. neoformans*-infected brain. We next evaluated the impact of CCR2 signaling on neuroinflammation. CCR2 deletion profoundly altered the expression of neuroinflammation genes from the NanoString multiplex panel (Fig. 5A). Specifically, CCR2 gene deletion reduced expressions of Th1 signature genes (*stat1*, *cxcl10*, *tnf*, *tnfrsr1a*, and *tnfrsr1b*), chemokines, and cytokines, as well as their receptors involved in myeloid and T cell recruitment and activation (CCL5, CCL12, CXCL6, CXCL10, CXCL11, CSF1R, CCR5, IL4RA, IL6RA), and an array of complement proteins (C1QA, C1QB, C1QC, C3, C4A) (Fig. 5A). Since IM were the only cell subset showing surface expression of CCR2, our data strongly suggest that IM were either directly or indirectly responsible for the expression of these genes within the CNS. We further studied how CCR2-deletion affected leukocyte populations other than IM during CM. We found profound changes in leukocyte composition (Fig. 5B) and an overall decrease in global leukocyte accumulation in the CNS throughout the observed time course of CM (Fig. 5C). While we detected no changes in the total number of microglia, CCR2 deficiency impaired the recruitment of CD4$^+$ T cells, CD8$^+$ T cells, and dendritic cells (DCs) but enhanced eosinophil accumulation in the brain (Fig. 5C to H). These results demonstrate that the CCR2 axis, presumably via its effects on IM, profoundly reduced the overall magnitude of CNS inflammation and altered its characteristics during CM.

CCR2 promotes pathological type 1 responses in the *C. neoformans*-infected brain. Strong Th1 T cell polarization and elevated levels of interferon gamma (IFN-γ) in the cerebrospinal fluid of CM patients are associated with neurological deterioration (31, 32). Our previous study also revealed a pathological role of the ultra-Th1 polarization in our highly inflammatory model of murine CM (12). While links between CCR2 axis and T cell polarization have been well documented in the lungs during *C. neoformans* infection (23, 30, 33), this has not been explored in the CNS. We found that the frequencies of T cells producing IFN-γ and tumor necrosis factor alpha (TNF-α; Th1) were reduced in the brain of CCR2$^{-/-}$ relative to those in the brain of WT mice (Fig. 6A and Fig. S6), while the frequencies of T cells producing interleukin 13 (IL-13; Th2), Foxp3 (Treg), and IL-17A (Th17) were increased (Fig. 6A and B). The absolute cell number of Th1 in the brain of CCR2$^{-/-}$ mice decreased compared to that in the brain of WT mice, but the numbers of Th2, Th17, and Tregs were comparable in both mouse strains (Fig. 6C). Interestingly, even in the absence of CCR2, Th1 still remained the dominant polarization type in CD4$^+$ T cells isolated from the CNS (Fig. 6B).

Th1 response stimulates myeloid cell classical activation, characterized by the expression of inducible nitric oxide synthase (iNOS) (25, 34). We found that more than 80% of IM in the WT mice produced high levels of iNOS at 21 dpi during CM (Fig. 6D and E), but only about 10% of microglia expressed iNOS (Fig. 6F and G). iNOS expression was ablated in CCR2$^{-/-}$ mice in both IM and microglia (Fig. 6D). In contrast, the IM and microglia in the brain of CCR2$^{-/-}$ mice expressed an increased level of arginase

FIG 4 Legend (Continued)
at 24 h posttransfer (right two panels). Representative flow cytometric dot plots are shown after CD11b$^+$Ly6C$^+$ IM gating. Numerical data or bar graphs showed mean ± SEM from an experiment representative of two to four independent experiments ($n > 3$). *, $P < 0.05$; **, $P < 0.01$; ***, $P < 0.001$.
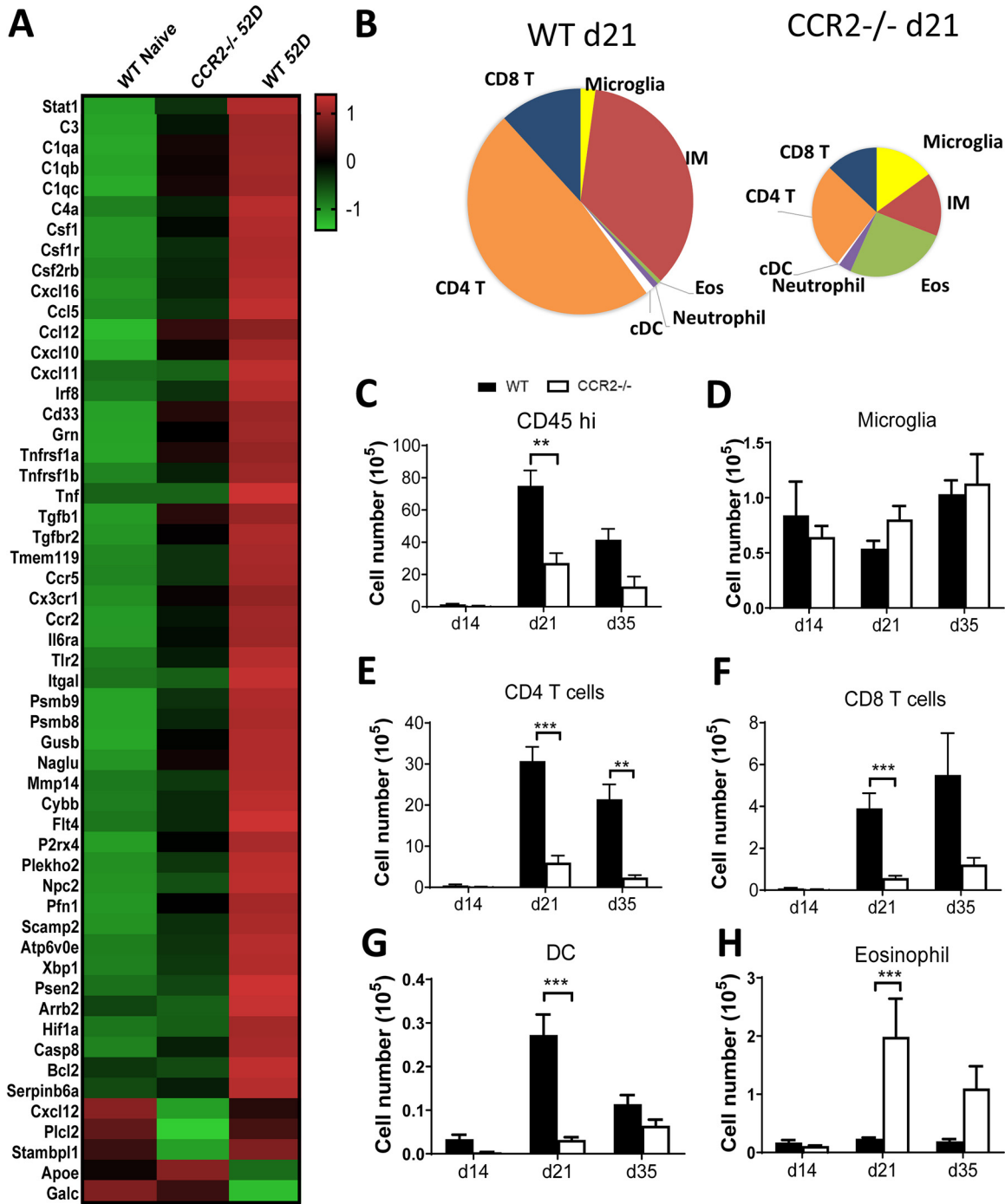
FIG 5 CCR2 modulates neuroinflammation during CM. (A) mRNA transcripts of immune-related genes in brain homogenate from naive WT, infected WT, and infected CCR2$^{-/-}$ were analyzed using a NanoString multiplex neuropathology panel. The results show normalized gene expression relative to housekeeping genes in the NanoString multiplex panel. $n = 3$ per group. Note significant upregulation of inflammatory genes in the WT mice at 21dpi and their minimal change in CCR2$^{-/-}$ mice. Frequencies (B) and total numbers of brain-infiltrating CD45^{hi} leukocytes (C), microglia (D), CD4$^+$ T cells (E), CD8$^+$ T cells (F), DC (G), and eosinophils (H) in brains of WT and CCR2$^{-/-}$ mice during CM. Mean $\pm$ SEM from an experiment representative of two to four independent experiments ($n > 4$). **, $P < 0.01$; ***, $P < 0.001$.

(ARG1) (Fig. 6D to G), an enzyme associated with an alternative-activation phenotype and nonfungicidal macrophages (35). Collectively, these data demonstrate that CCR2 plays a role in the development of the pathological ultra Th1 response and the subsequent strong M1 polarization within the CNS during CM.
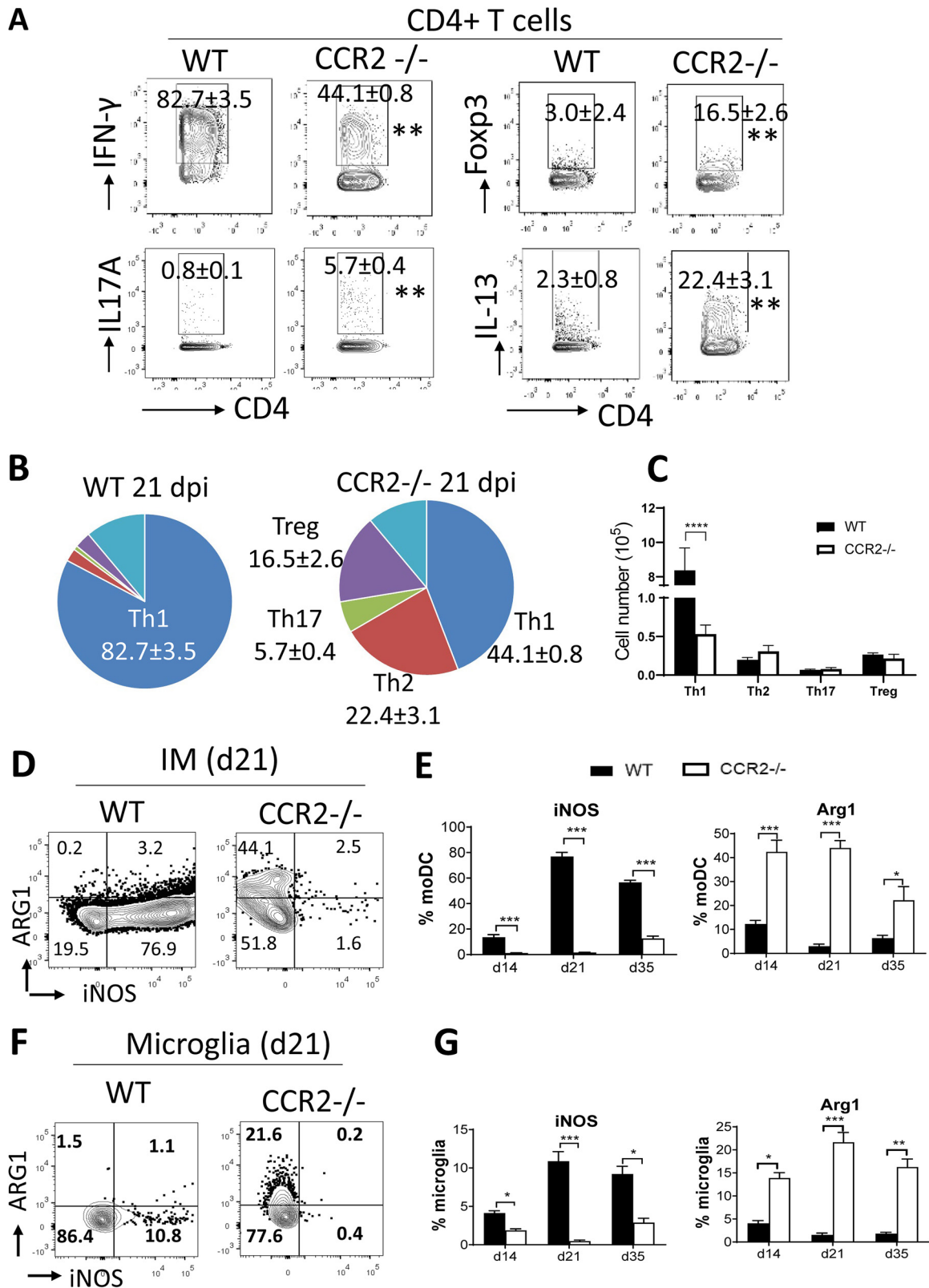
A

B

C

D

E

F

G

FIG 6 CCR2 contributes to pathological type 1 inflammation during *C. neoformans* brain infection. (A and B) Frequencies of CD4$^+$ T cells producing IFN-γ, IL-17A, Foxp3, and IL-13 isolated from the brains of WT and CCR2$^{-/-}$ mice 21 dpi show a shift in the immune polarization away from the ultra-Th1 response toward a more-balanced, mixed Th-phenotype in CCR2$^{-/-}$ mice during CM. The pie charts show the ratio of different subsets of CD4$^+$ T cells, Th1 (IFN-γ^+), Th2 (IL-13$^+$), Th17 (IL-17A$^+$), Tregs (Foxp3$^+$), and other cells without detectable cytokine productions. (C) Total cell numbers of CD4$^+$ T cells subsets isolated from the brains of WT and CCR2$^{-/-}$

(Continued on next page)

DISCUSSION

Evidence is accumulating to support the pivotal role of neuroinflammation in CM pathogenesis (36). In the current study, we demonstrate that (i) CM mortality and neurological deterioration are marked by neuronal cell death and dysfunction in the areas infiltrated by the inflammatory cells, (ii) CCR2 plays a critical role in driving both neuroinflammation and the lethal pathology despite promoting fungal clearance, (iii) while affecting multiple cell subsets, CCR2 was critically required for the recruitment of inflammatory monocytes (IM, CD45^{hi}CD11b$^+$Ly6C$^+$) into the brain during CM, and (iv) CCR2 contributed to the accumulation of polarized Th1 CD4$^+$ T cells, propelling the highly pathological ultra-Th1 immune response within the *C. neoformans*-infected brain. Together, our study demonstrates an essential role of the CCR2 signaling in modulating CNS inflammation and driving neuronal pathology.

Apart from the short-term neurological deterioration of CM patients (6), persistent neuropsychological deficits are increasingly recognized upon their recovery from the severe CM (6, 37–40). Even with successful fungal eradication, CM patients exhibit overall rates of neuropsychological deficits higher than standardized population norms (37–40). Elevated cerebrospinal fluid (CSF) neurofilament light chains (NFL), a marker of axonal damage, were detected in human patients and suggested ongoing neurological damage (6), but detailed molecular mechanisms of brain pathology during CM are lacking. Here, using a new approach to reduce the inflammatory response (by CCR2 deletion) in CM mice, in addition to our previous two approaches (T cell depletion and CXCR3 deletion) (12, 13), we clearly show that rather than the fungus itself, the host inflammatory response is responsible for the development of lethal CNS damage. For the first time, however, we performed a detailed analysis of transcriptional pathways linked to the CNS pathology using a NanoString panel designed for studies of neurological disorders. Compared to those of healthy brains, we found highly significant changes in global neurotransmission and neuroinflammation pathways. We found these alterations to be specifically concentrated around the leukocyte-infiltrated cryptococcal lesions using confocal microscopy. The most striking finding was that most of these pathological changes could be alleviated or even reversed upon the CCR2 deletion, which resulted in profoundly reduced inflammatory infiltration of the affected areas of the brain. These improvements at the molecular level corresponded to the improved behavioral readouts and the health status of the CCR2$^{-/-}$ CM mice. While our study only begins to "zoom into" the specific groups of CNS genes that are altered during CM, future studies looking into the human homolog gene subset and correlating them with the clinical outcomes will help to identify the CM patients at the greatest risk of inflammatory brain damage. Stratifying patients into groups that require appropriate immunomodulatory therapies will guide rationalized treatment of CM patients and likely those with other CNS infections.

Immune responses in the delicate CNS need to be especially well balanced to control the infectious agents while also minimizing immune-mediated CNS damage (7, 36, 41, 42). CCL2 was previously identified as one of the major chemokines detected in the CSF of patients with HIV-associated CM and was associated with the risk for the development of life-threatening immune reconstitution inflammatory syndrome (IRIS) (19). Our study establishes a mechanistic link between CCL2/CCR2 pathway and brain pathology by demonstrating that CCR2 contributes to the development of neurological symptoms and mortality. Because targeting CCR2 or monocytes is a proposed strategy for targeted therapy in cancer, steatohepatitis, traumatic brain injury, Alzheimer's disease, and multiple sclerosis (43–48), our work suggests that targeting this pathway might offer clinical benefits to patients with inflammatory CNS disease.

FIG 6 Legend (Continued)

mice at 21 dpi. (D and E) Expressions of iNOS and ARG1 by IM were analyzed in the brain of WT and CCR2$^{-/-}$ mice by intracellular flow cytometry. Note that IM produce a high level of iNOS in infected WT but shift to express ARG1 in infected CCR2$^{-/-}$ mice. (F and G) iNOS and ARG1 expression by microglia isolated from brains of WT and CCR2$^{-/-}$ mice with CM. Mean ± SEM from an experiment representative of two to four independent experiments ($n > 4$). *, $P < 0.05$; **, $P < 0.01$; ***, $P < 0.001$.

CCL2/CCR2 axis regulates the mobilization of monocytes from bone marrow to the inflammatory sites (21). CD14^{hi}CD16-monocytes predominate in the CSF during CM (9), but their function and migration mechanisms are still not well understood. Here, we demonstrate that their murine equivalent, CCR2$^+$CD11b$^+$Ly6C$^+$ IM, is the dominant myeloid cell subset in the brain of the cryptococcal-infected brains. The CCR2 deletion leads to reduced monocyte accumulation in the spleen, suggesting a defect in monocyte egress from the bone marrow as previously reported (21). Our adoptive transfer study showed that CCR2-positive monocytes migrate from the bloodstream into the CNS more efficiently than the CCR2-deficient monocytes. Therefore, CCR2 plays a role in mediating monocyte crossing the blood-brain barrier during CM, even though other pathways appear to be also involved at this stage. Together, both of these CCR2-dependent IM recruitment steps accounted for roughly 95% of their CNS recruitment at the peak of the inflammation time point in our CM model.

We previously showed that CXCR3$^+$IFN-γ^+ CD4$^+$ T cells are required for disease pathology during CM (13). However, the T cells at the peripheral tissues require to be restimulated by the specific antigen-loaded APCs to perform their effector functions (49). In cryptococcal pulmonary infection, CCR2-dependent IM colocalization with CD4$^+$ T cells in the bronchovascular infiltrates and promotes the local Th1 responses (23). Here, we demonstrate that CCR2-deletion leads to decreased accumulation and Th1-polarized CD4$^+$ T cells in the brain but does not alter the magnitude of other Th-subsets during CM. Improved neurological symptoms in CCR2$^{-/-}$ mice provide a clue that CCR2$^+$ IM work hand-in-hand with CD4$^+$ T cells to drive disease pathology. However, future studies are needed to determine whether IM work predominately as the recruiters and activators of the pathological T cells, as the pathological effectors directly inducing neuronal damage upon activation by the Th1 cells, or as contributors to both processes as described in other models of inflammatory CNS damage. The IM and T cell cross talk in jointly mediating pathology has been described in cerebral malaria and experimental autoimmune encephalomyelitis models, pointing out the critical role of T cell/IM interactions under different disease conditions (50–52). One hint regarding the possible direct pathological role of the IM is their strong classical activation status in the WT mice and CCR2 deficiency dramatically shifting their profile to an alternatively activated phenotype. The excessive activation of IM has been linked to tissue pathology in neurological diseases (17).

While the role of CCR2 in our CM model seems to be predominately linked to IM recruitment, CCR2 was reported to be expressed by other cells, such as Th17 and Treg in different disease models (53, 54). However, in our model, these mechanisms are unlikely to be at play since we find no detectable surface expression of CCR2 on cells other than IM, and CCR2 deletion has not affected recruitment of Th17 and Treg into the *C. neoformans*-infected brain.

Regarding translational value, our murine model uses an intravenous (i.v.) injection with a clinical isolate from a human patient (ATCC 24067, 52D), which is sufficiently virulent to establish a highly reproducible, controlled-onset mouse model of CM in the immunocompetent mice (12). As expected, these mice developed adaptive immune responses that aid fungal clearance but unfortunately with severe to lethal collateral damage. In human patients, most cryptococcal infections/expansion are predominantly caused by a weak immune system, which correlates with high brain fungal load and poor prognosis. However, many AIDS patients with very high CFU in their CSF exhibit relatively few symptoms and often have a better prognosis than those with CM without known immune impairment. In early time points of infection in the WT mice and through the observed time course in CCR2$^{-/-}$ mice, we see high fungal burdens but very few neurological symptoms and relatively little inflammation. With the development of CNS inflammation in the WT mice, severe pathologies were developed in the CNS before we could observe any direct effects of the fungal pathogen. Thus, our model resembles outcomes in patients with severe refractory CM or those who developed c-IRIS. Our results may provide important insights into the immune pathogenesis

and guidance for the development and use of pro- versus anti-inflammatory therapies to minimize CNS injury. Our results imply that too-rapid immune-boosting treatments may not be beneficial or could be harmful in some patients with CM and suggest that the CM patients' inflammatory status (including levels of CCR2 ligands) within CNS should be monitored and appropriately "toned" therapeutically.

One limitation of our model is that the i.v.-injected strain grown on Sabouraud dextrose broth bypasses pulmonary defenses and *in vivo* changes that *Cryptococcus* normally undergoes before brain infection, and another is that the strain 52D falls in a midrange of virulence compared to many other clinical isolates that are more virulent. Whether and how these factors affect CNS inflammation and pathology will need to be investigated.

In summary, we found that CCR2 orchestrates lethal immune pathology despite its important role in fungal clearance during CM. CCR2 promotes the recruitment of IM into the brain and strongly modulates neuroinflammation during CM. Targeting the CCR2 pathway and IM may create new therapeutic opportunities as an adjunct therapy for CM, especially those with uncontrolled CNS inflammation.

MATERIALS AND METHODS

Mice. Male and female C57BL/6J mice were obtained from Jackson Laboratories (Bar Harbor, ME). CCR2$^{-/-}$ mice (55) backcrossed to C57BL/6J were housed under specific-pathogen-free conditions in the Animal Care Facility at the VA Ann Arbor Healthcare System. Mice were 8 to 12 weeks old at the time of infection and were humanely euthanized by CO_2 inhalation at the time of data collection. All experiments were approved by the Veterans Affairs Institutional Animal Care and Use Committee under protocol 1408-004 and were performed following NIH guidelines and the Guide for the Care and Use of Laboratory Animals. Data presented were from both male and female mice, and no significant differences in CFU, MCBS, survival, and CNS cell accumulation between animal sexes were found during *C. neoformans* brain infection.

C. neoformans. ATCC 24067 (American Type Culture Collection, Manassas, VA), *C. neoformans* strain 52D was recovered from 10% glycerol frozen stocks and grown for 96 h at 37°C in Sabouraud dextrose broth (1% Neopeptone, 2% dextrose; Difco, Detroit, MI) on a shaker. The cultures were then centrifuged and the pellets were washed with phosphate-buffered saline (PBS). Cells were counted via hemocytometer and diluted to a concentration of 5×10^6/ml just before infection. Mice were infected with 10^6 organisms (in 200 μl PBS) via retro-orbital intravenous injection under inhaled isoflurane anesthesia. Serial dilutions of the *C. neoformans* suspension were plated on Sabouraud dextrose agar to confirm the number of viable fungi in the inoculum.

Murine coma and behavioral scale. A murine coma and behavioral scale (MCBS) was used to assess the overall physical and neurological condition of infected mice as described previously (12, 13). In brief, mice were scored using a scale of 0 to 3 for exploration, balance, gait, body posture, coat condition, grip strength, reflexes (body, neck, pinna, and footpad reflexes), and response to visual stimuli. Lower scores reflect more-pronounced symptoms.

Fungal burdens. The total fungal burden was qualified on a per organ basis. Samples of brains and spleens homogenate were serially diluted with distilled water. Aliquots of each sample (10 μl) were plated on Sabouraud dextrose in duplicates. The CFU of the samples were counted after 48 h.

Brain leukocyte isolation. Leukocytes in the brain were isolated as described previously (12). Briefly, mice were euthanized with CO_2 and then perfused with PBS to remove circulating red blood cells and leukocytes from the brain. The brains were then aseptically removed, transferred to GentleMACs C tubes containing 5 ml of digest medium (RPMI 1640 with 5% fetal bovine serum [FBS], 25 mM HEPES, GlutaMAX, penicillin-streptomycin, nonessential amino acids, sodium pyruvate, and beta-mercaptoethanol, collagenase [50 μg/ml; Roche], and DNase [100 U/ml; Worthington]). The tissue was minced and then processed on a GentleMACs homogenizer (Miltenyi). The homogenate was washed with RPMI 1640 and filtered through a 70-μm cell strainer. A discontinuous 30%/70% Percoll (GE Healthcare) gradient was used to remove cell debris, myelin, and neurons, and then microglia and brain-infiltrating leukocytes (BIL) were recovered from the interface. Isolated cells were then washed twice with PBS. Total cell numbers were determined by counting live cells on a hemocytometer with trypan blue.

Flow cytometry. After isolation, cells were stained with fixable live/dead dye (Life Technologies), blocked with anti-CD16/32, and stained with antibodies for CD45 (30-F11), CD3 (145-2C11), CD4 (GK1.5), CD8 (53-6.7), CD11b (M1/70), CD11c (N418), Ly6C (HK1.4), F4/80 (BM8), CD64 (X54-5/7.1), XCR1 (ZET), SIRPα (P84), and/or major histocompatibility complex class II (MHCII, M5/114.15.2).

For intracellular iNOS and ARG1 production by myeloid cells, the cells were stained for extracellular markers and then fixed and permeabilized with 2% formaldehyde for 30 min. Intracellular staining for iNOS (CXNFT) and ARG1 (IC5868P, R&D SYSTEMS) was performed in the permeabilization buffer.

For intracellular cytokine production by T cells, the cells were stimulated for 6 h with phorbol myristate acetate and ionomycin in the presence of brefeldin A and monensin for the final 4 h. The cells were stained for extracellular markers and then fixed with fixation/permeabilization buffer, and intracellular staining for Foxp3 and IFN-γ was performed in permeabilization buffer. Fluorescence minus one (FMO)

controls were used for all experiments. Data were collected on either an LSRII cytometer (BD) or an LSRFortessa (BD) and were analyzed using FlowJo (TreeStar).

NanoString analysis. Total RNA was isolated from the whole-brain homogenate using TRIzol (Life Technologies) and sent for NanoString nCounter analysis (NanoString Technologies) (56). Briefly, target RNA was labeled with a capture probe and a reporter probe specific to the genes of interest. After hybridization, the probe-target complexes were immobilized on an imaging surface and then scanned by a fluorescence microscope. Data analysis was performed on the nSolver analysis software according to the manufacturer's instructions and built-in statistical analyses. Pathway scores were calculated as the first principal component of the pathway genes' normalized expression. The software will orient the scores such that increased score corresponds with increased expression in a majority of the pathway genes. Scores of the cell type characteristic genes were analyzed using the default settings from the cell type profiling algorithm in the nSolver analysis software.

Microscopy. Sections were deparaffinized in xylene and gradually rehydrated by a gradient of alcohol to water. Antigen retrieval was carried out in citrate buffer on a boiling water bath for 15 min. Sections were blocked in 5% bovine serum albumin (BSA) in PBS. For the beta III tubulin and synaptotagmin-7 staining, sections were stained with a rabbit polyclonal beta III antibody (1:100, Abcam) and synaptotagmin-7 antibody (clone S275, Invitrogen) for 1 h at 37°C. Secondary antibody staining was done with goat anti-mouse Alexa 555 antibody and goat anti-rabbit Alexa 488 antibody (1:500, Invitrogen) for 45 min at 37°C. For the beta III tubulin and cleaved caspase-3 stainings, sections were then stained with primary antibody to beta III tubulin (TuJ1) and a rabbit antibody specific to cleaved caspase-3 (1:100, Sigma) for 1 h at 37°C. Sections were then washed in PBS and counterstained with a secondary goat anti-mouse secondary Alexa 647 antibody and goat anti-rabbit Alexa 555 secondary antibody (1:500) for 45 min at 37°C. After that, the sections were washed in PBS for 30 min. The autofluorescence was quenched by Vector's true view kit (Vector Laboratories) as per the manufacturer's protocol before mounting with mounting medium. Samples were visualized using a KEYENCE microscope BZ-X800 series. Images were captured by the camera provided by the vendor by using a ×20 objective 0.45 numerical aperture (NA) Nikon. Images were deconvolved for enhancing the clarity of the images. Images were analyzed by ImageJ, and the numbers of damaged neurons were calculated by counting the numbers of cleaved caspase-3 positive neurons around the area infected by *Cryptococcus*. Areas that are 500 square microns around the cryptococcal lesions were analyzed. All the images were captured under the same settings.

***In vivo* monocyte adoptive transfer.** Bone marrow from CD45.1 WT and CD45.2 CCR2$^{-/-}$ mice were harvested as previously described (57, 58). Monocytes were isolated using EasySep mouse monocyte isolation kit (STEMCELL Technologies) according to the manufacturer's instructions. Wild-type and CCR2-deficient cells were mixed (2.5×10^6 each per mouse) and coinjected via retro-orbital intravenous injection in 200 μl of PBS into CD45.1 × CD45.2 mice at 20 dpi. The brains were harvested and brain leukocytes were isolated and analyzed by flow cytometry 24 h after adoptive transfer.

Cytokine expression. Cytokine levels were measured from the supernatants of whole-brain homogenate after centrifugation ($600 \times g$, 5 min) using LegendPlex cytometric bead assays (BioLegend) according to the manufacturer's instructions.

Statistical analysis. Statistical analysis was performed using GraphPad Prism version 6 software with Student's *t* test or analysis of variance (ANOVA) plus Tukey's *post hoc* test for multiple comparisons. Asterisks on figures (in graphs or in the corners of flow cytometry plots) indicate statistical significance as follows: *, $P < 0.05$; **, $P < 0.01$; ***, $P < 0.001$; ****, $P < 0.0001$.

SUPPLEMENTAL MATERIAL

Supplemental material is available online only.

FIG S1, PDF file, 0.2 MB.
FIG S2, PDF file, 0.1 MB.
FIG S3, PDF file, 0.4 MB.
FIG S4, PDF file, 0.2 MB.
FIG S5, PDF file, 0.1 MB.
FIG S6, PDF file, 0.1 MB.

REFERENCES

1. Rajasingham R, Smith RM, Park BJ, Jarvis JN, Govender NP, Chiller TM, Denning DW, Loyse A, Boulware DR. 2017. Global burden of disease of HIV-associated cryptococcal meningitis: an updated analysis. Lancet Infect Dis 17:873–881. https://doi.org/10.1016/S1473-3099(17)30243-8.

2. Williamson PR, Jarvis JN, Panackal AA, Fisher MC, Molloy SF, Loyse A, Harrison TS. 2017. Cryptococcal meningitis: epidemiology, immunology, diagnosis and therapy. Nat Rev Neurol 13:13–24. https://doi.org/10.1038/nrneurol.2016.167.

3. Perfect JR, Dismukes WE, Dromer F, Goldman DL, Graybill JR, Hamill RJ, Harrison TS, Larsen RA, Lortholary O, Nguyen M-H, Pappas PG, Powderly WG, Singh N, Sobel JD, Sorrell TC. 2010. Clinical practice guidelines for the management of cryptococcal disease: 2010 update by the Infectious Diseases Society of America. Clin Infect Dis 50:291–322. https://doi.org/10.1086/649858.

4. Pyrgos V, Seitz AE, Steiner CA, Prevots DR, and, Williamson PR. 2013. Epidemiology of cryptococcal meningitis in the US: 1997–2009. PLoS One 8: e56269. https://doi.org/10.1371/journal.pone.0056269.

5. Naik KR, Saroja AO, and, Doshi DK. 2017. Hospital-based retrospective study of cryptococcal meningitis in a large cohort from India. Ann Indian Acad Neurol 20:225–228. https://doi.org/10.4103/aian.AIAN_39_17.

6. Panackal AA, Wuest SC, Lin Y-C, Wu T, Zhang N, Kosa P, Komori M, Blake A, Browne SK, Rosen LB, Hagen F, Meis J, Levitz SM, Quezado M, Hammoud D, Bennett JE, Bielekova B, Williamson PR. 2015. Paradoxical immune responses in non-HIV cryptococcal meningitis. PLoS Pathog 11: e1004884. https://doi.org/10.1371/journal.ppat.1004884.

7. Panackal AA, Williamson KC, van de Beek D, Boulware DR, Williamson PR. 2016. Fighting the monster: applying the host damage framework to human central nervous system infections. mBio 7:e01906-15. https://doi.org/10.1128/mBio.01906-15.

8. Meya DB, Manabe YC, Boulware DR, and, Janoff EN. 2016. The immunopathogenesis of cryptococcal immune reconstitution inflammatory syndrome-understanding a conundrum. Curr Opin Infect Dis 29:10–22. https://doi.org/10.1097/QCO.0000000000000224.

9. Meya DB, Okurut S, Zziwa G, Rolfes MA, Kelsey M, Cose S, Joloba M, Naluyima P, Palmer BE, Kambugu A, Mayanja-Kizza H, Bohjanen PR, Eller MA, Wahl SM, Boulware DR, Manabe YC, Janoff EN. 2015. Cellular immune activation in cerebrospinal fluid from Ugandans with cryptococcal meningitis and immune reconstitution inflammatory syndrome. J Infect Dis 211:1597–1606. https://doi.org/10.1093/infdis/jiu664.

10. Boulware DR, Meya DB, Muzoora C, Rolfes MA, Huppler Hullsiek K, Musubire A, Taseera K, Nabeta HW, Schutz C, Williams DA, Rajasingham R, Rhein J, Thienemann F, Lo MW, Nielsen K, Bergemann TL, Kambugu A, Manabe YC, Janoff EN, Bohjanen PR, Meintjes G. 2014. Timing of antiretroviral therapy after diagnosis of cryptococcal meningitis. N Engl J Med 370:2487–2498. https://doi.org/10.1056/NEJMoa1312884.

11. Jarvis JN, Bicanic T, Loyse A, Namarika D, Jackson A, Nussbaum JC, Longley N, Muzoora C, Phulusa J, Taseera K, Kanyembe C, Wilson D, Hosseinipour MC, Brouwer AE, Limmathurotsakul D, White N, van der Horst C, Wood R, Meintjes G, Bradley J, Jaffar S, Harrison T. 2014. Determinants of mortality in a combined cohort of 501 patients with HIV-associated Cryptococcal meningitis: implications for improving outcomes. Clinical Infectious Diseases 58:736–745. https://doi.org/10.1093/cid/cit794.

12. Neal LM, Xing E, Xu J, Kolbe JL, Osterholzer JJ, Segal BM, Williamson PR, and, Olszewski MA. 2017. CD4+ T cells orchestrate lethal immune pathology despite fungal clearance during Cryptococcus neoformans meningoencephalitis. mBio 8:e01415-17. https://doi.org/10.1128/mBio.01415-17.

13. Xu J, Neal LM, Ganguly A, Kolbe JL, Hargarten JC, Elsegeiny W, Hollingsworth C, He X, Ivey M, Lopez R, Zhao J, Segal B, Williamson PR, Olszewski MA. 2020. Chemokine receptor CXCR3 is required for lethal brain pathology but not pathogen clearance during cryptococcal meningoencephalitis. Sci Adv 6: eaba2502. https://doi.org/10.1126/sciadv.aba2502.

14. Meya DB, Okurut S, Zziwa G, Cose S, Boulware DR, and, Janoff EN. 2019. HIV-associated Cryptococcal immune reconstitution inflammatory syndrome is associated with aberrant t cell function and increased cytokine responses. J Fungi 5:42. https://doi.org/10.3390/jof5020042.

15. Khaw YM, Aggarwal N, Barclay WE, Kang E, Inoue M, and, Shinohara ML. 2020. Th1-dependent cryptococcus-associated immune reconstitution inflammatory syndrome model with brain damage. Front Immunol 11:529219. https://doi.org/10.3389/fimmu.2020.529219.

16. Codarri L, Greter M, Becher B. 2013. Communication between pathogenic T cells and myeloid cells in neuroinflammatory disease. Trends Immunol 34:114–119. https://doi.org/10.1016/j.it.2012.09.007.

17. Croxford AL, Lanzinger M, Hartmann FJ, Schreiner B, Mair F, Pelczar P, Clausen BE, Jung S, Greter M, and, Becher B. 2015. The cytokine GM-CSF drives the inflammatory signature of CCR2+ monocytes and licenses autoimmunity. Immunity 43:502–514. https://doi.org/10.1016/j.immuni.2015.08.010.

18. Mildner A, Mack M, Schmidt H, Brück W, Djukic M, Zabel MD, Hille A, Priller J, Prinz M. 2009. CCR2+ Ly-6Chi monocytes are crucial for the effector phase of autoimmunity in the central nervous system. Brain 132:2487–2500. https://doi.org/10.1093/brain/awp144.

19. Jarvis JN, Meintjes G, Bicanic T, Buffa V, Hogan L, Mo S, Tomlinson G, Kropf P, Noursadeghi M, Harrison TS. 2015. Cerebrospinal fluid cytokine profiles predict risk of early mortality and immune reconstitution inflammatory syndrome in HIV-associated cryptococcal meningitis. PLoS Pathog 11:e1004754. https://doi.org/10.1371/journal.ppat.1004754.

20. Barber DL, Andrade BB, Sereti I, Sher A. 2012. Immune reconstitution inflammatory syndrome: the trouble with immunity when you had none. Nat Rev Microbiol 10:150–156. https://doi.org/10.1038/nrmicro2712.

21. Chu HX, Arumugam TV, Gelderblom M, Magnus T, Drummond GR, Sobey CG. 2014. Role of CCR2 in inflammatory conditions of the central nervous system. J Cereb Blood Flow Metab 34:1425–1429. https://doi.org/10.1038/jcbfm.2014.120.

22. Osterholzer JJ, Chen G-H, Olszewski MA, Curtis JL, Huffnagle GB, Toews GB. 2009. Accumulation of CD11b+ lung dendritic cells in response to fungal infection results from the CCR2-mediated recruitment and differentiation of Ly-6Chigh monocytes. J Immunol 183:8044–8053. https://doi.org/10.4049/jimmunol.0902823.

23. Osterholzer JJ, Curtis JL, Polak T, Ames T, Chen G-H, McDonald R, Huffnagle GB, Toews GB. 2008. CCR2 mediates conventional dendritic cell recruitment and the formation of bronchovascular mononuclear cell infiltrates in the lungs of mice infected with Cryptococcus neoformans. J Immunol 181:610–620. https://doi.org/10.4049/jimmunol.181.1.610.

24. Zhang Y, Wang F, Bhan U, Huffnagle GB, Toews GB, Standiford TJ, Olszewski MA. 2010. TLR9 signaling is required for generation of the adaptive immune protection in Cryptococcus neoformans-infected lungs. Am J Pathol 177:754–765. https://doi.org/10.2353/ajpath.2010.091104.

25. Leopold CW, Hole CR, Wozniak KL, Olszewski MA, Wormley JF. 2014. STAT1 signaling is essential for protection against Cryptococcus neoformans infection in mice. J Immunol 193:4060–4071. https://doi.org/10.4049/jimmunol.1400318.

26. Heung LJ, Hohl TM. 2019. Inflammatory monocytes are detrimental to the host immune response during acute infection with Cryptococcus neoformans. PLoS Pathog 15:e1007627. https://doi.org/10.1371/journal.ppat.1007627.

27. Hsieh CL, Niemi EC, Wang SH, Lee CC, Bingham D, Zhang J, Cozen ML, Charo I, Huang EJ, Liu J, Nakamura MC. 2014. CCR2 deficiency impairs macrophage infiltration and improves cognitive function after traumatic brain injury. J Neurotrauma 31:1677–1688. https://doi.org/10.1089/neu.2013.3252.

28. Tian D-S, Peng J, Murugan M, Feng L-J, Liu J-L, Eyo UB, Zhou L-J, Mogilevsky R, Wang W, Wu L-J. 2017. Chemokine CCL2–CCR2 signaling induces neuronal cell death via STAT3 activation and IL-1β production after status epilepticus. J Neurosci 37:7878–7892. https://doi.org/10.1523/JNEUROSCI.0315-17.2017.

29. Schumak B, Klocke K, Kuepper JM, Biswas A, Djie-Maletz A, Limmer A, van Rooijen N, Mack M, Hoerauf A, Dunay IR. 2015. Specific depletion of Ly6Chi inflammatory monocytes prevents immunopathology in

experimental cerebral malaria. PLoS One 10:e0124080. https://doi.org/10.1371/journal.pone.0124080.

30. Traynor TR, Kuziel WA, Toews GB, and, Huffnagle GB. 2000. CCR2 expression determines T1 versus T2 polarization during pulmonary Cryptococcus neoformans infection. J Immunol 164:2021–2027. https://doi.org/10.4049/jimmunol.164.4.2021.

31. Boulware DR, Bonham SC, Meya DB, Wiesner DL, Park GS, Kambugu A, Janoff EN, Bohjanen PR. 2010. Paucity of initial cerebrospinal fluid inflammation in cryptococcal meningitis is associated with subsequent immune reconstitution inflammatory syndrome. J Infect Dis 202:962–970. https://doi.org/10.1086/655785.

32. Haddow LJ, Colebunders R, Meintjes G, Lawn SD, Elliott JH, Manabe YC, Bohjanen PR, Sungkanuparph S, Easterbrook PJ, French MA, Boulware DR, International Network for the Study of HIV-associated IRIS (INSHI). 2010. Cryptococcal immune reconstitution inflammatory syndrome in HIV-1-infected individuals: proposed clinical case definitions. Lancet Infect Dis 10:791–802. https://doi.org/10.1016/S1473-3099(10)70170-5.

33. Qiu Y, Zeltzer S, Zhang Y, Wang F, Chen G-H, Dayrit J, Murdock BJ, Bhan U, Toews GB, Osterholzer JJ, Standiford TJ, Olszewski MA. 2012. Early induction of CCL7 downstream of TLR9 signaling promotes the development of robust immunity to cryptococcal infection. J Immunol 188:3940–3948. https://doi.org/10.4049/jimmunol.1103053.

34. Aguirre K, Gibson G. 2000. Differing requirement for inducible nitric oxide synthase activity in clearance of primary and secondary Cryptococcus neoformans infection. Med Mycol 38:343–353. https://doi.org/10.1080/714030965.

35. Rodriguez PC, Ochoa AC, Al-Khami AA. 2017. Arginine metabolism in myeloid cells shapes innate and adaptive immunity. Front Immunol 8:93. https://doi.org/10.3389/fimmu.2017.00093.

36. Pirofski L-a, Casadevall A. 2017. Immune-mediated damage completes the parabola: Cryptococcus neoformans pathogenesis can reflect the outcome of a weak or strong immune response. mBio 8:e02063-17. https://doi.org/10.1128/mBio.02063-17.

37. Nakajima H, Takayama A, Fujiki Y, Ito T, Kitaoka H. 2015. Refractory Cryptococcus neoformans meningoencephalitis in an immunocompetent patient: paradoxical antifungal therapy-induced clinical deterioration related to an immune response to cryptococcal organisms. Case Rep Neurol 7:204–208. https://doi.org/10.1159/000440948.

38. Brizendine KD, Baddley JW, Pappas PG. 2013. Predictors of mortality and differences in clinical features among patients with Cryptococcosis according to immune status. PLoS One 8:e60431. https://doi.org/10.1371/journal.pone.0060431.

39. Traino K, Snow J, Ham L, Summers A, Segalà L, Shirazi T, Biassou N, Panackal A, Anjum S, Marr KA, Kreisl WC, Bennett JE, Williamson PR. 2019. HiV-negative cryptococcal Meningoencephalitis results in a persistent frontal-Subcortical Syndrome. Sci Rep 9:1–9. https://doi.org/10.1038/s41598-019-54876-7.

40. Chen C-H, Chang C-C, Chang W-N, Tsai N-W, Lui C-C, Lin W-C, Chen N-C, Chen C, Huang C-W, Lu C-H. 2012. Neuro-psychological sequelae in HIV-negative cryptococcal meningitis after complete anti-fungal treatment. Acta Neurol Taiwan 21:8–17.

41. Skerrett SJ, Park DR. 2001. Anti-inflammatory treatment of acute and chronic pneumonia. Semin Respir Infect 16:76–84. https://doi.org/10.1053/srin.2001.22731.

42. Bicanic T, Meintjes G, Rebe K, Williams A, Loyse A, Wood R, Hayes M, Jaffar S, Harrison T. 2009. Immune reconstitution inflammatory syndrome in HIV-associated cryptococcal meningitis: a prospective study. J Acquir Immune Defic Syndr 51:130–134. https://doi.org/10.1097/QAI.0b013e3181a56f2e.

43. Lim SY, Yuzhalin AE, Gordon-Weeks AN, Muschel RJ. 2016. Targeting the CCL2-CCR2 signaling axis in cancer metastasis. Oncotarget 7:28697–28710. https://doi.org/10.18632/oncotarget.7376.

44. Li X, Yao W, Yuan Y, Chen P, Li B, Li J, Chu R, Song H, Xie D, Jiang X, Wang H. 2017. Targeting of tumour-infiltrating macrophages via CCL2/CCR2 signalling as a therapeutic strategy against hepatocellular carcinoma. Gut 66:157–167. https://doi.org/10.1136/gutjnl-2015-310514.

45. Noel MS, Hezel AF, Linehan D, Wang-Gillam A, Eskens F, Sleijfer S, Desar I, Erdkamp F, Wilmink J, Diehl J, Potarca A, Zhao N, Deng J, Lohr L, Miao S, Charo I, Singh R, Schall TJ, Bekker P. 2017. Orally administered CCR2 selective inhibitor CCX872-b clinical trial in pancreatic cancer. J Clin Oncol 35:276. https://doi.org/10.1200/JCO.2017.35.4_suppl.276.

46. Fani Maleki A, and, Rivest S. 2019. Innate immunity as a therapeutic target for Alzheimer's disease and multiple sclerosis. Front Cell Neurosci 13:355. https://doi.org/10.3389/fncel.2019.00355.

47. Parker R, Walters M, Ertl L, Ebsworth K, Tan J, McMahon J, Powers J, Adams D, Jaen J, and, Schall T. 2014. Therapeutic use of a clinical stage CCR2 inhibitor, CCX872, in obesity-associated steatohepatitis. Lancet 383:S78. https://doi.org/10.1016/S0140-6736(14)60341-X.

48. Morganti JM, Jopson TD, Liu S, Riparip L-K, Guandique CK, Gupta N, Ferguson AR, Rosi S. 2015. CCR2 antagonism alters brain macrophage polarization and ameliorates cognitive dysfunction induced by traumatic brain injury. J Neurosci 35:748–760. https://doi.org/10.1523/JNEUROSCI.2405-14.2015.

49. Lindell DM, Moore TA, McDonald RA, Toews GB, Huffnagle GB. 2006. Distinct compartmentalization of CD4+ T-cell effector function versus proliferative capacity during pulmonary cryptococcosis. Am J Pathol 168:847–855. https://doi.org/10.2353/ajpath.2006.050522.

50. Hirako IC, Ataide MA, Faustino L, Assis PA, Sorensen EW, Ueta H, Araújo NM, Menezes GB, Luster AD, Gazzinelli RT. 2016. Splenic differentiation and emergence of CCR5+ CXCL9+ CXCL10+ monocyte-derived dendritic cells in the brain during cerebral malaria. Nat Commun 7:13277. https://doi.org/10.1038/ncomms13277.

51. Izikson L, Klein RS, Charo IF, Weiner HL, Luster AD. 2000. Resistance to experimental autoimmune encephalomyelitis in mice lacking the CC chemokine receptor (CCR2). J Exp Med 192:1075–1080. https://doi.org/10.1084/jem.192.7.1075.

52. Clarkson BD, Walker A, Harris MG, Rayasam A, Sandor M, Fabry Z. 2015. CCR2-dependent dendritic cell accumulation in the central nervous system during early effector experimental autoimmune encephalomyelitis is essential for effector T cell restimulation in situ and disease progression. J Immunol 194:531–541. https://doi.org/10.4049/jimmunol.1401320.

53. Brühl H, Cihak J, Schneider MA, Plachý J, Rupp T, Wenzel I, Shakarami M, Milz S, Ellwart JW, Stangassinger M, Schlöndorff D, Mack M. 2004. Dual role of CCR2 during initiation and progression of collagen-induced arthritis: evidence for regulatory activity of CCR2+ T cells. J Immunol 172:890–898. https://doi.org/10.4049/jimmunol.172.2.890.

54. Kara EE, McKenzie DR, Bastow CR, Gregor CE, Fenix KA, Ogunniyi AD, Paton JC, Mack M, Pombal DR, Seillet C, Dubois B, Liston A, MacDonald KPA, Belz GT, Smyth MJ, Hill GR, Comerford I, McColl SR. 2015. CCR2 defines in vivo development and homing of IL-23-driven GM-CSF-producing Th17 cells. Nat Commun 6:8644. https://doi.org/10.1038/ncomms9644.

55. Kuziel WA, Morgan SJ, Dawson TC, Griffin S, Smithies O, Ley K, Maeda N. 1997. Severe reduction in leukocyte adhesion and monocyte extravasation in mice deficient in CC chemokine receptor 2. Proc Natl Acad Sci U S A 94:12053–12058. https://doi.org/10.1073/pnas.94.22.12053.

56. Geiss GK, Bumgarner RE, Birditt B, Dahl T, Dowidar N, Dunaway DL, Fell HP, Ferree S, George RD, Grogan T, James JJ, Maysuria M, Mitton JD, Oliveri P, Osborn JL, Peng T, Ratcliffe AL, Webster PJ, Davidson EH, Hood L, Dimitrov K. 2008. Direct multiplexed measurement of gene expression with color-coded probe pairs. Nat Biotechnol 26:317–325. https://doi.org/10.1038/nbt1385.

57. Arora S, Olszewski MA, Tsang TM, McDonald RA, Toews GB, and, Huffnagle GB. 2011. Effect of cytokine interplay on macrophage polarization during chronic pulmonary infection with Cryptococcus neoformans. Infect Immun 79:1915–1926. https://doi.org/10.1128/IAI.01270-10.

58. Xu J, Flaczyk A, Neal LM, Fa Z, Eastman AJ, Malachowski AN, Cheng D, Moore BB, Curtis JL, Osterholzer JJ, Olszewski MA. 2017. Scavenger receptor MARCO orchestrates early defenses and contributes to fungal containment during cryptococcal infection. J Immunol 198:3548–3557. https://doi.org/10.4049/jimmunol.1700057.